

**NASA TECHNICAL  
MEMORANDUM**

NASA TM X-71636

NASA TM X-71636

(NASA-TM-X-71636) EFFECT OF ANODE RING  
ARRANGEMENT ON THE SPECTROSCOPIC  
CHARACTERISTICS OF THE NASA LEWIS BUMPY  
TORUS PLASMA (NASA) 18 p HC \$3.25

N75-13627

Unclas  
03666

CSSL 201 G3/75

**EFFECT OF ANODE RING ARRANGEMENT ON THE  
SPECTROSCOPIC CHARACTERISTICS OF THE  
NASA LEWIS BUMPY TORUS PLASMA**

by Richard W. Richardson  
Lewis Research Center  
Cleveland, Ohio 44135



TECHNICAL PAPER presented at  
Sixteenth Annual Meeting of the Plasma Physics  
Division of the American Physical Society  
Albuquerque, New Mexico, October 28-31, 1974

EFFECT OF ANODE RING ARRANGEMENT ON THE  
SPECTROSCOPIC CHARACTERISTICS OF THE  
NASA LEWIS BUMPY TORUS PLASMA

by Richard W. Richardson\*

Lewis Research Center

ABSTRACT

E-8177

The modified Penning discharge in the NASA Lewis Bumpy Torus is normally produced by an anode ring at high voltage in each of the 12 magnetic mirror midplanes. For this investigation, the plasma was run with 12, 6, 3, and 1 anode rings. When 3 anode rings were used, the spectroscopically determined relative electron density and mean ion residence time increase by factors of 10 and 5, respectively, in one mode of operation. The discharge is observed to uniformly fill all bumps around the torus regardless of the anode arrangement and number. A plasma density on axis of  $10^{11} \text{ cm}^{-3}$  is estimated for the 3 anode case in one mode of operation based on an observed discharge current to ion loss rate correlation and a measured mean ion residence time of .5 msec.

INTRODUCTION

A hot-ion plasma is produced in the NASA Lewis Bumpy Torus confinement geometry by a steady-state Penning discharge (ref. 1). Normally, the discharge has been operated with an anode ring at high positive potential in each of the 12 magnetic mirror midplanes. Spectroscopic measurement of electron temperature, relative electron density, and ion residence time has been recently reported (ref. 2) for a wide range of operating conditions in a helium

---

\*NASA-NRC Postdoctoral Associate

plasma with the 12 anode configuration.

For the series of measurements to be reported here, the discharge has been operated with some anode rings removed to see if there is a pronounced effect on plasma properties and discharge characteristics. A series of experimental runs have been performed in helium gas with 12, 6, 3, and 1 anode rings. The electron temperature, relative electron density, and ion residence time have been determined from the spectroscopic measurements.

## EXPERIMENT

### Apparatus

The NASA Lewis Bumpy Torus magnet facility (refs. 3 and 4) consists of 12 superconducting coils arranged in a toroidal array as shown in fig. 1. The mirror ratio is 2.5:1 and the maximum magnetic field is 3.0 Tesla. The major diameter of the torus is 1.52 meters. An 18 cm diameter anode ring is normally placed at each magnetic mirror midplane. A steady-state discharge is maintained between the grounded coils and tank walls and the anodes biased to a high positive potential. The individual anode rings can be disconnected from the high voltage and retracted from the discharge region (see fig. 1). This capability has been used to perform a preliminary series of runs with 12, 6, 3, and 1 anode rings. In the case of 6 and 3 anode rings, rings were placed in every other and every fourth bump, respectively. In the case of one anode ring, the discharge was operated with the anode in different locations around the torus. Ion temperatures, normally measured by a charge-exchange neutral detector, were not taken for this preliminary series of runs.

### Operating Conditions

For this series of measurements, the discharge was operated in helium to facilitate the spectroscopic measurements as was done in previous work (ref. 2). Voltage-current characteristics obtained with 12 anode rings are

shown in fig. 2 with the neutral helium background pressure,  $p_o$ , as parameter. The discharge is observed to operate in two distinctly different modes, the low pressure mode (LPM) and high pressure mode (HPM) as shown in fig. 2. Although the voltage-current characteristics were quantitatively somewhat different for the different anode configurations, the mode structure persisted (ref. 5). The discharge was observed for the same set of operating conditions in each mode for the different anode configurations. The LPM condition was at an anode voltage,  $V_A$ , of 20.0 kV and  $p_o = 2.8 \times 10^{-5}$  Torr. The HPM condition was  $V_A = 7.0$  kV and  $p_o = 8.3 \times 10^{-5}$  Torr. The discharge current,  $I$ , at these conditions was a function of the number of anode rings,  $N$ , and the anode ring configuration and is shown in fig. 3. The numbers in parenthesis by each data point in fig. 3 specify the location of the anode rings according to the legend. In both modes the discharge current is observed to increase from  $N = 12$  to  $N = 3$ . With one anode, the current is dependent on which location the anode occupies. This is most pronounced in the LPM where a factor of ten change in current is observed between anode positions number, 7 and 4. With a single anode, the current was somewhat sensitive to anode alignment but not enough to entirely account for the observed behavior. With  $N \geq 3$  the current was found to be reproducible on removal and replacement of the anodes. For  $N = 6$  and 3 the current was independent of anode ring position.

### Measurement of Spectral Intensities

The spectroscopic set-up was identical to that reported in ref. 2. The relative intensities of the 504.8 nm and 471.3 nm helium spectral lines emitted from the plasma were viewed across horizontal chords in the magnetic mirror midplane at position 7 (see fig. 3). For all anode configurations, the plasma was observed at the same location. In the case of twelve anode rings and one of the anode ring runs, an anode occupies the midplane being observed. The remaining runs with  $N = 1$  and the  $N = 6$  and 3 runs were made with no anode ring at the mirror midplane of the spectroscopic observation. For each anode configuration, the intensity and shape of the discharge was observed visually to be

quite similar between all mirrors including those with and without anode rings. For this reason, it is believed that data at the single midplane observed can be considered representative of the entire discharge regardless of the anode ring configuration.

When the plasma was viewed spectroscopically with an anode ring at the observed midplane, the plasma filled the volume inside the anode ring and had a distinct boundary at the inside edge of the anode ring. When viewing with no anode ring, the bulk of the visible plasma was inside the original anode ring radius, however, viewing across a chord, low level linearly decreasing light intensity was observed outside the original anode ring radius. In some cases, the low level light continued outside the field of view of the optics. In these cases, the light intensity was extrapolated linearly with radius to zero in order to allow Abel inversion. Assuming radial symmetry, a forty point Abel inversion routine (ref. 6) was used to obtain relative radial emission coefficient profiles,  $\epsilon'_j(r)$ , for each line from the chord averaged line intensities at 40 equally spaced vertical distances from the minor axis of the torus.

## INTERPRETATION OF SPECTROSCOPIC DATA

### Determination of Electron Temperature and Density

Assuming a weakly ionized corona model plasma, the emission coefficient,  $\epsilon_j(r)$ , of a spectral line,  $j$ , at a radius  $r$  from the minor axis of the torus is given by

$$\epsilon_j(r) = k\epsilon'_j(r) = n(r)n_0 S_j [T_e(r)] \text{ cm}^3 \text{ sec}^{-1} \quad (1)$$

In this equation  $n(r)$  is the electron density,  $n_0$  is the background neutral density,  $S_j(T_e)$  is the apparent optical line excitation rate coefficient for excitation from the neutral ground state assuming a Maxwellian electron energy,  $T_e$  is the corresponding electron temperature,  $k$  is the absolute calibration factor of the optical system and  $\epsilon'_j(r)$  is the measured relative emission coefficient (the relative spectral calibration is included in  $\epsilon'_j$ ). Since the  $S_j$  for the 504.8 nm

and 471.3 nm spectral lines have dissimilar electron temperature dependences, the ratio of the measured emission coefficients

$$\frac{\epsilon'_{504.8}}{\epsilon'_{471.3}} = \frac{S_{504.8}(T_e)}{S_{471.3}(T_e)} \quad (2)$$

can be used to determine  $T_e$  (ref. 2, 7). The apparent optical cross sections discussed in ref. 2 have been used to calculate the  $S_j$  as a function of  $T_e$  and to determine  $T_e(r)$ .

Using one of the measured  $\epsilon'_j$ , equation (1), and the measured  $T_e$  one can determine the relative electron density  $n'(r)$  from the relation

$$n'(r) = \frac{n(r)}{k} = \frac{\epsilon'_j(r)}{n_0 S_j[T_e(r)]} \quad (3)$$

The helium neutral density,  $n_0$ , is determined from  $p_0$  as measured by an ion gauge away from the discharge assuming a uniform  $n_0$  through the discharge. This relative electron density is useful for determining radial profiles and variations with operating conditions and anode configurations. For the range of electron temperatures in this device (10-200 eV) the rate coefficients,  $S_j(T_e)$ , are not extremely steep functions of  $T_e$  as for temperatures less than 10 eV. Thus, the uncertainty in  $n'$  which results from small uncertainty in  $T_e$  is acceptable for the range of operating temperatures.

#### Determination of Ion Residence Time

Assuming charge neutrality and dominant wall recombination, a continuity equation can be written for the ions in this discharge of the form

$$\frac{\partial \bar{n}(\vec{r})}{\partial t} + \vec{\nabla} \cdot \vec{\Gamma}(\vec{r}) = \bar{n}(\vec{r}) n_0 S_I[T_e(\vec{r})] \quad (4)$$

where  $r$  is a position in the toroidal volume,  $\vec{\Gamma}$  is the ion flux at  $r$ , and  $S_I(T_e)$  is the ground state ionization rate coefficient for Maxwellian electrons on neu-

trals (ref. 8). Since this is a steady-state discharge, the first term in equation 4 is zero. Integrating equation 4 over the plasma volume,  $V_p$ , and using the divergence theorem gives

$$\int_{A_p} \vec{\Gamma} \cdot \vec{n} \, dA = \int_{V_p} n(\vec{r}) n_o S_I [T_e(\vec{r})] dV \quad \text{sec}^{-1} \quad (5)$$

where  $\vec{n}$  is the normal to the plasma surface and  $A_p$  is the area of the plasma. A mean ion residence time,  $\tau_i$ , can be defined by writing the loss term on the right hand side of equation 5 in the form

$$\int_{A_p} \vec{\Gamma} \cdot \vec{n} \, dA \equiv \frac{\int_{V_p} n(\vec{r}) dV}{\tau_i} \quad (6)$$

in which case

$$\tau_i \equiv \frac{\int_{V_p} n(\vec{r}) dV}{\int_{V_p} n(\vec{r}) n_o S_I [T_e(\vec{r})] dV} \quad \text{sec} \quad (7)$$

The ion residence time,  $\tau_i$ , is interpreted as the mean time between the production of an electron-ion pair and the eventual loss of the ion from the plasma, which is rigorously true if the electron temperature is uniform through the plasma. Assuming the spectroscopic data taken at the midplane is representative of the entire discharge, equation 7 can be approximated by

$$\tau_i \approx \tau_i' = \frac{\int_{V_m} n'(\vec{r}) dV}{\int_{V_m} n'(\vec{r}) n_o S_I [T_e(\vec{r})] dV} \quad \text{sec} \quad (8)$$

where the integrals are evaluated numerically from the measured radial profiles at the midplane and  $V_m$  is the observed midplane volume. The approximate time is used to evaluate the variation of the ion residence time of the plasma.

### Discharge Current Relationship

The magnet coil bores (which constitute the cathode potential surfaces nearest the plasma) are outside the magnetic flux lines which define the outside edge of the plasma (see fig. 4). The current path to the cathode may be completed across the plasma cathode gap by ions lost from the plasma while only electrons are collected by the anode rings. This is expected because the ion gyroradius in this hot-ion plasma is much larger than that of the electrons and of the order of the gap distance. Secondary electrons emitted from the cathode are more likely to be collected directly along field lines to the anode support shafts which are at anode potential. Any current to the anode supports would constitute a parasitic current in parallel to the current passing through the plasma. If this concept is valid, the equation

$$\frac{I_p}{e} = \int_{V_p} \bar{n}(\vec{r}) n_o S_I [T_e(\vec{r})] dV \quad \text{sec}^{-1} \quad (9)$$

should hold where  $I_p$  is the plasma current (discharge current  $I$  minus parasitic currents flowing external to the plasma), and  $e$  is the charge of an electron. Equation 9 states that all particle loss contributes to plasma current. This is expected to be so since there are no non-current collecting (floating or insulating) surfaces near the discharge (surfaces which would be expected to collect a particle flux but no net current). In order to investigate the validity of equation 9 the right hand side can be approximately calculated from the spectroscopic results. The integral over the entire volume is approximated by the numerical integration of the experimental radial profiles,  $\int_{V_m} \bar{n}' n_o S_I (T_e) dV$ , at the midplane. This relative quantity can be plotted versus  $I$  to investigate the functional dependence of equation 9. Assuming the parasitic currents are small, then equations 9 and 7 can be combined to estimate the volume averaged density,  $\bar{n}$ , assuming  $\tau_i \approx \tau_i'$ . In this case

$$\bar{n} = \frac{I \tau_i'}{e V_p} \quad \text{cm}^{-3} \quad (10)$$

where  $\bar{n} = \frac{1}{V_p} \int_{V_p} n(\vec{r}) dV$  and  $V_p = 82 \times 10^3 \text{ cm}^3$  is the volume defined by the intersection of the magnetic flux lines with the inside edge of the anode rings.

## RESULTS AND DISCUSSION

### Radial Profiles

Radial profiles of the electron density normalized to its value on axis (except for LPM,  $N = 12$  as noted) are shown in figs. 5 and 6 for the HPM and LPM, respectively, for different  $N$ . In the HPM (fig. 5) the profiles are observed to be similar for cases  $N = 12, 6,$  and  $3$  except for the sharp boundary at the anode ring for  $N = 12$ . With  $N = 6$  and  $3$ , the sharp boundary at the anode edge was visually observed to persist in those bumps with an anode. With  $N = 1$ , the discharge was visually observed to be much more diffuse, extending well beyond the anode ring radius, as seen in the radial profile of fig. 5. For the LPM (fig. 6) the results are similar to the HPM except for the pronounced increase in density near the anode at the observation midplane for  $N = 12$ , typical of previous investigation of the LPM. The central structure of the discharge is seen to be similar for  $N = 12, 6,$  and  $3$ . For  $N = 1$ , in the LPM the discharge again becomes quite diffuse as can be seen from the profiles. Only one representative radial profile for  $N = 1$  is shown for each mode.

### Ion Residence Time

The ion residence times,  $\tau_i$ , were calculated from equation 8 using the radial profiles. Results are shown in fig. 7 as a function of  $N$  for both modes. Also indicated for each point is the corresponding mean electron temperature,  $\overline{T_e}$ . The estimated error bars for the HPM are large due to the steepness of the ionization rate curve at the lower electron temperatures. The increase in  $\tau_i$  in the HPM to  $500 \mu\text{sec}$  when going to  $N = 3$  is quite pronounced as well as the decrease when going to  $N = 1$ . In the LPM,  $\tau_i$  is essentially independent of  $N$  within the estimated error for  $N = 12, 6,$  and  $3$ . The error bars have been

suppressed for the  $N = 1$  data due to the small scale and crowding of points, but are the same as for the other LPM points. The scatter of the  $N = 1$  points is apparently due to the pronounced difference in the discharge as reflected in the discharge current (see fig. 3) depending on which location is occupied by an anode. The energy loss times appropriate for Lawson parameter calculation are generally much shorter than  $\tau_i$  in this helium discharge since charge-exchange collisions are more probable than ion loss, ref. 5.

### Relative Electron Density

Plots of the relative electron density,  $n'(0)$ , on axis as obtained from the Abel inversion and equation 3 (used for normalization in figs. 5 and 6) are shown in fig. 8 for the HPM and LPM as a function of  $N$ . The density in the HPM is observed to increase by more than a factor of ten when going from  $N = 12$  to  $N = 3$  followed by a decrease for  $N = 1$ . In the LPM for  $N = 12$ , if the density on axis were replaced by the peak density which occurs near the anode (see fig. 6) the densities for  $N = 2, 6,$  and  $3$  would be the same within the estimated error. For both modes and  $N = 1$ , the density is strongly dependent on which location the anode ring occupies. Visual observation indicates that this density is representative of the entire discharge.

### Discharge Current Correlation

In fig. 9,  $\int V_m n' n_o S_I(T_e) dV$  is plotted as a function of the discharge current,  $I$ . Figure 9 shows that over two orders of magnitude, this quantity is proportional to  $I$  to within roughly a factor of two for both discharge modes and various number of anodes. This includes the six erratically varying sets of points for  $N = 1$ , as well as the  $N = 12, 6,$  and  $3$  cases. This proportionality has also been observed to hold in the LPM for a much wider range of operating conditions in the same helium discharge (ref. 2) with  $N = 12$  where the density and ion residence time were obtained from simple chord averages. A systematic variation from the proportionality was observed in ref. 2 for the HPM per-

haps due to the chord average which is not evidenced here. The existence of this experimental functional relationship lends support to the validity of equation 10, but does not establish its quantitative equality.

The existence of the proportionality does allow consideration of the question as to how much of the discharge current actually flows through the toroidal plasma. Large, independent parasitic currents flowing outside the discharge volume (cathode secondaries collected by the anode support or current due to independent discharges occurring away from the toroidal discharge) would be expected to spoil the correlation of fig. 9. A result of the correlation is then that these parasitic currents are either small or a fixed percentage of the toroidal plasma current within the factor of two spread in fig. 9.

### Absolute Electron Density

Assuming that to a reasonable degree of approximation equation 10 holds, the absolute density can be estimated using the  $\tau_i'$  measured at the midplane. This gives for the case of highest relative density (HPM and  $N = 3$ )  $\bar{n} \cong 4 \times 10^{10} \text{ cm}^{-3}$ . Consideration of the effect of the volume average from the midplane radial profiles leads to an estimated density on axis of  $n(0) \cong 10^{11} \text{ cm}^{-3}$ . This can at best be considered an order of magnitude estimate of the density in light of the discussions concerning (9) and (10) in the previous section. The density is approaching that which can be measured by the 70 Ghz microwave interferometer installed on the device. Direct measurements of the density and comparison with the density determined from equation 7 will be of great value in determining the validity of equation 9 and the spectroscopic results.

### One Anode Ring Configuration

The observations with one anode ring were generally found not to be consistent with observed trends for  $N = 12$  to 3 and not consistent from one location to another. The observations were found to be consistent with the other measurements only through the correlation of fig. 9. With  $N = 6$  and 3, the gross

operating conditions were found to be grossly insensitive to which locations the three or six anode rings occupied, unlike the one anode ring cases. The reason for the anomalous behavior with  $N = 1$  is not known. It was found that with one anode the discharge current was somewhat sensitive to alinement. Perhaps with three or more rings alinement of the individual rings becomes less important. In the past, on removing and replacing the normal 12 anodes, no difficulty was encountered in reproducing conditions. The condition of the individual anode ring and nearby surfaces may be important as well as small geometrical differences between the different mirrors which would also tend to average out with more rings. Aside from the erratic behavior with  $N = 1$ , the plasma conditions were found in all cases to be less desirable than for  $N = 12$  to 3.

There was no obvious reason (based on visual observation) to believe that the spectroscopic results were affected by the relation of the mirror viewed to the mirror occupied by an anode ring either in the case of  $N = 1$  or  $N = 12$  to 3. This does need to be investigated further in a quantitative manner.

### Discharge Mechanism

For all cases, as has been discussed, the discharge was observed visually to fill all mirrors around the torus, the plasma volume defined essentially at the midplanes by the anode ring radius from the minor axis. Other work (ref. 9) has indicated the toroidal plasma floats to near anode potential. These two observations are consistent with the picture that the electric fields, resulting from the potential drop between the plasma ring and grounded walls, penetrate the plasma, heating and sustaining the discharge. This allows the discharge to operate in mirrors without an anode ring. The anode ring apparently serves primarily to bias the plasma ring to high potential.

### CONCLUDING REMARKS

The spectroscopic measurements obtained during this preliminary study indicate significant increases in density and ion residence times in the HPM on

reducing the number of anode rings from twelve to three. Operation with one anode alone does not, however, produce desirable conditions. The measurements indicate that the LPM is insensitive to anode configuration. Operation with less than 12 anodes may present technical advantages such as allowing easier anode alignment, less arcing, and less parasitic current losses.

Over the wide range of geometrical and operating conditions, the discharge current was found to be proportional to the ion production rate. An absolute measurement of the density would perhaps establish the equality and thus allow a simple direct measure of the ion loss rate from the discharge current.

General visual observation of the discharge has suggested that the discharge is sustained by electric fields perpendicular to magnet flux lines, the potential being coupled from mirror to mirror along magnetic flux lines.

#### REFERENCES

1. Roth, J. R.; Richardson, R. W.; and Gerdin, G. A.: Initial Results from the NASA Lewis Bumpy Torus Experiment. Presented at the American Physical Society, Annual Meeting, Philadelphia, Pa., Oct. 30-Nov. 4, 1973.
2. Richardson, R. W.: Spectroscopic Results in Helium from the NASA Lewis Bumpy Torus Plasma. Presented at the First Intern. Conf. on Plasma Sci., Knoxville, Tenn., May 15-17, 1974.
3. Roth, J. R.; Holmes, A. D.; Keller, T. A.; and Krawczonek, W. M.: Characteristics and Performance of a Superconducting Bumpy Torus Magnet Facility for Plasma Research. NASA TN-D-7353, 1973.
4. Roth, J. R.; Holmes, A. D.; Keller, T. A.; and Krawczonek, W. M.: A 12-Coil Superconducting "Bumpy Torus" Magnet Facility for Plasma Research In: Applied Superconductivity Conf., 5th Annapolis, Md., May 1-3, 1972, pp. 361-366.
5. Roth, J. R.: Ion Heating and Containment in the NASA Lewis Bumpy Torus Plasma, NASA TM X, October 1974.

6. Lochte-Holtgreven, W., ed.: Plasma Diagnostics. North Holland Publishing Co., 1968, pp. 184-186.
7. Sovie, R. J.: Spectroscopic Determination of Electron Temperature and Percentage Ionization in a Helium Plasma. Phys. Fluids, vol. 7, Apr. 1964, pp. 613-614.
8. Lotz, W.: Electron Impact Ionization Cross-Sections and Ionization Rate Coefficients for Atoms and Ions from Hydrogen to Calcium. Zeit. Fur Phys., vol. 216, no. 3, 1968, pp. 241-247.
9. Gerdin, G. A.: Spoke Wavenumbers and Mode Transitions in the NASA Lewis Bumpy Torus. Presented at Sixteenth Annual Meeting of the Plasma Physics, American Physical Society, Albuquerque, New Mexico, Oct. 28-31, 1974.

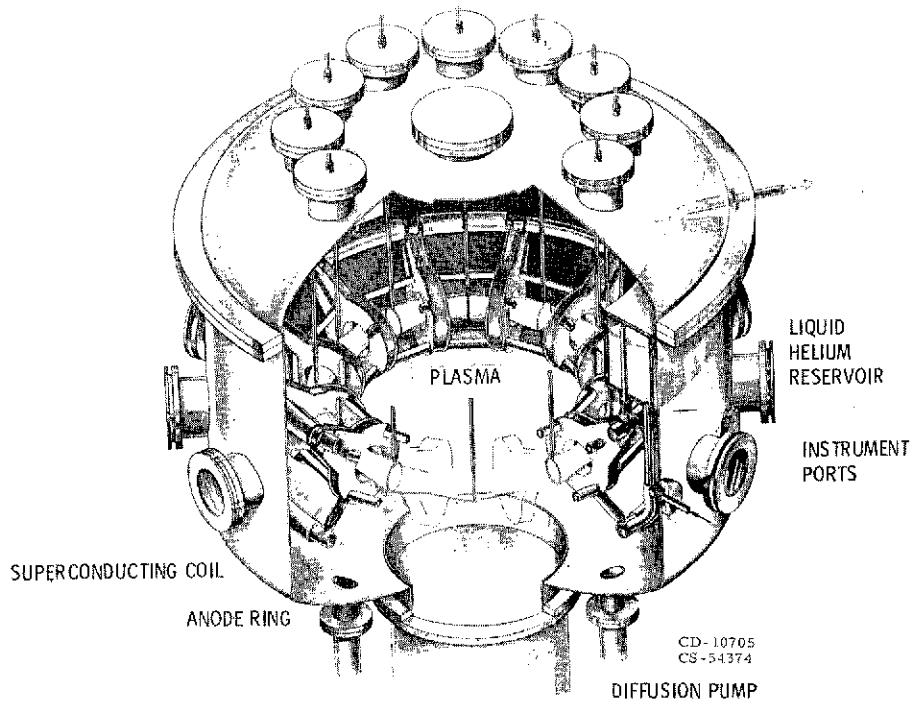


Figure 1. - Schematic of bumpy torus magnetic confinement geometry.

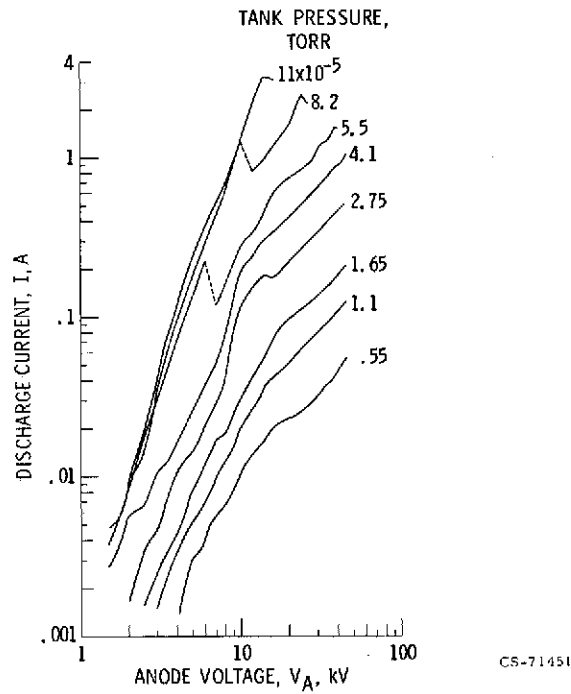


Figure 2. - Voltage current characteristics for discharge in pure helium and  $B_{MAX} = 2.4$  T.

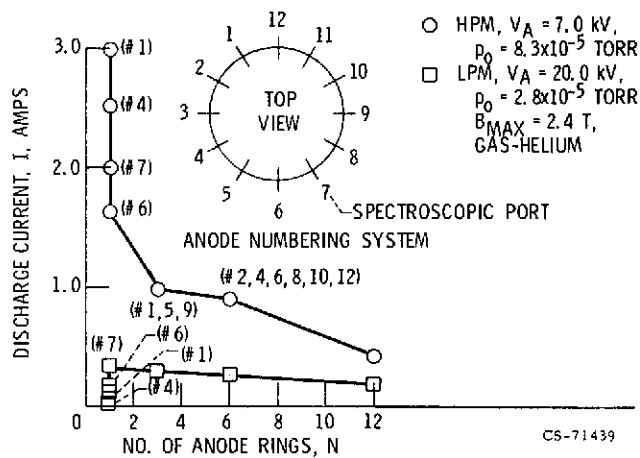


Figure 3. - Discharge current with various anode configurations for two modes of operation.

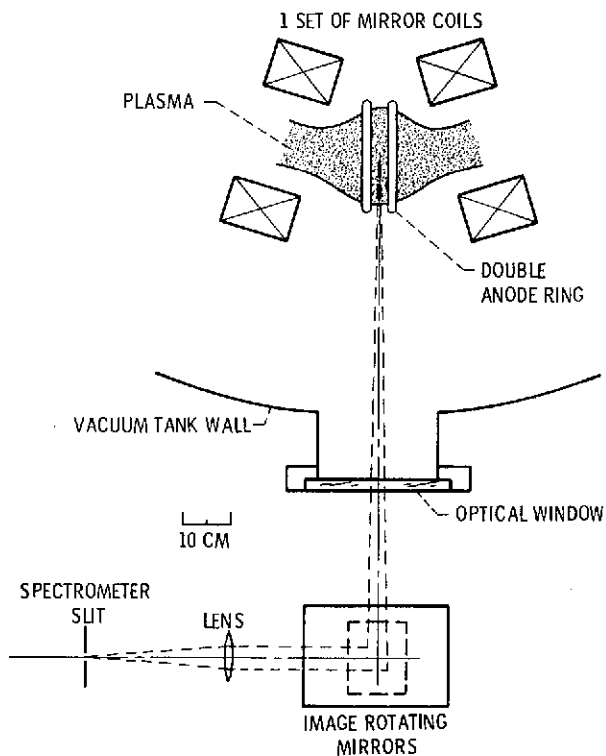


Figure 4. - Schematic drawing of the spectroscopic apparatus used to take electron temperature, relative electron number density, and radial profiles of these quantities.

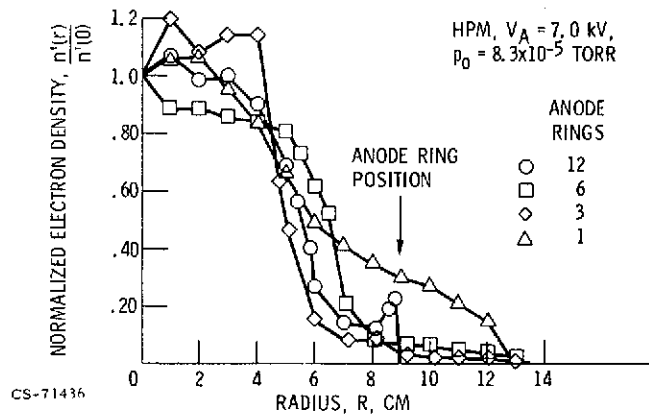


Figure 5. - Normalized electron density radial profiles in HPM.

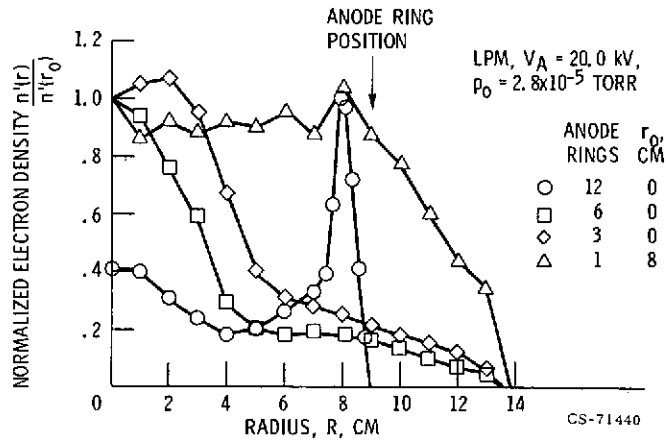


Figure 6. - Normalized electron density radial profiles in LPM.

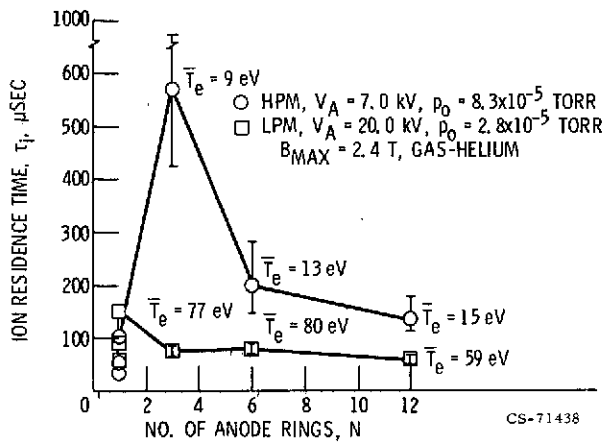


Figure 7. - Variation of mean ion residence time with various anode configurations.

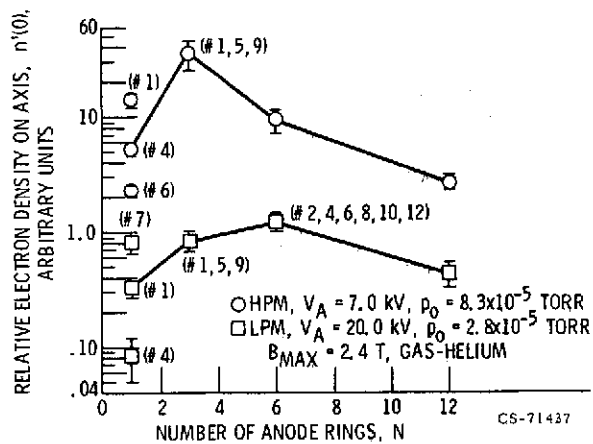


Figure 8. - Variations of electron density on axis with anode configuration.

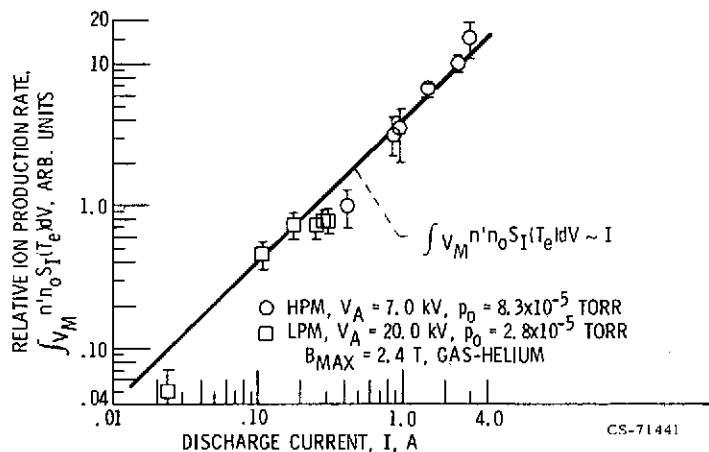


Figure 9. - Correlation between relative ion production rate and discharge current.